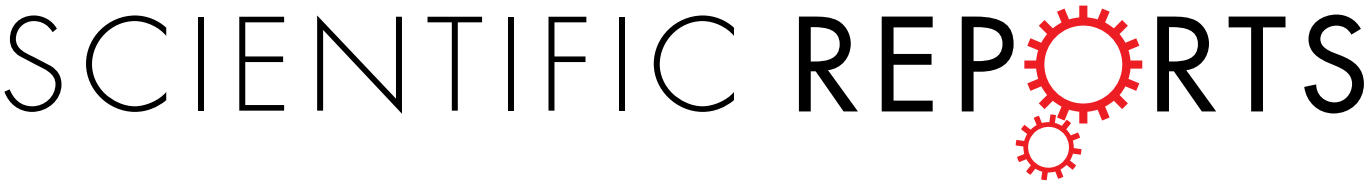

OPEN

Microporous carbons derived from melamine and isophthalaldehyde: One-pot condensation and activation in a molten salt medium for efficient gas adsorption

Received: 29 January 2018
Accepted: 21 March 2018
Published online: 17 April 2018

Adeela Rehman & Soo-Jin Park

In the present work, mixture of melamine and isophthalaldehyde undergo simultaneous polymerization, carbonization, and *in situ* activation in the presence of molten salt media through a single all-in-one route to design microporous carbons with high specific surface areas (~3000 m^2/g). The effect of the activation temperature and molten salts on the polymerization process and final texture of the carbon was explored. Carbon materials prepared at 700 °C, in the presence of KOH (referred as MIK-700), exhibited a narrower pore-size distribution ~1.05 nm than those prepared in the presence of the eutectic KOH-NaOH mixture (MIKN). Additionally, MIK-700 possesses an optimum micropore volume (1.33 cm^3/g) along with a high nitrogen content (2.66 wt%), resulting in the excellent CO_2 adsorption capacity of 9.7 mmol/g at 273 K and 1 bar. Similarly, the high specific area and highest total pore volume play an important role in H_2 storage at 77 K, with 4.0 wt% uptake by MIKN-800 (specific surface area and pore volume of 2984 m^2/g and 1.98 cm^3/g, respectively.) Thus, the facile one-step solvent-free synthesis and activation strategy is an economically favorable avenue for designing microporous carbons as an efficient gas adsorbents.

The energy costs related to the separation and sanitization of industrial commodities, such as gases, currently presents approximately 15% of global energy production, and the requirement of such commodities is anticipated to be triple by 2050[1]. Today the need of innovating effective separation and purification methods with lesser energy footprints is more for carbon dioxide (CO_2) than for any other gas. This is probably due to its contribution to climate change as well as the contamination of other gas streams including natural gas, biogas and syngas[2]. Apart from CO_2 adsorption and separation, the storage of H_2, a next-generation energy carrier with a high chemical energy (39 kW h/kg) and ability to provide pollution-free ignition is also need of the present time. Recently, porous carbons are considered as an emerging candidates as H_2 storage materials by virtue of their facile preparation, low cost, light weight, fast kinetics, and high surface area[3,4].

Different methods have been reported to fabricate microporous carbon materials with a high surface area[5–7]. Microporosity and high nitrogen content render Schiff-base polymers a highly interesting class of materials for the synthesis of carbons via pyrolysis. For the polymer synthesis, an organic media is used as the solvent for the reaction between primary amines as nucleophilic center and electrophilic carbons of the carbonyl groups to synthesize the polymer framework[8,9]. The resulting carbons obtained by the pyrolysis of the polymers possess a moderate surface area of 500–1500 m^2/g which can be improved further using KOH as the chemical activating agent. Although chemical activation by KOH is a widely used technique to produce a porous network[10], the number of variables in the experimental parameters and the differences in the reactivity of precursors limits a comprehensive understanding of the mechanism. In general, the reaction between carbon and KOH begins with the solid–solid interaction followed by the solid–liquid reaction which may reduce the potassium compound to metallic potassium (K), oxidize carbon to carbon oxides and carbonates accompanied by the formation of various

Department of Chemistry, Inha University, 100 Inharo, Incheon, 22212, Korea. Correspondence and requests for materials should be addressed to S.-J.P. (email: sjpark@inha.ac.kr)

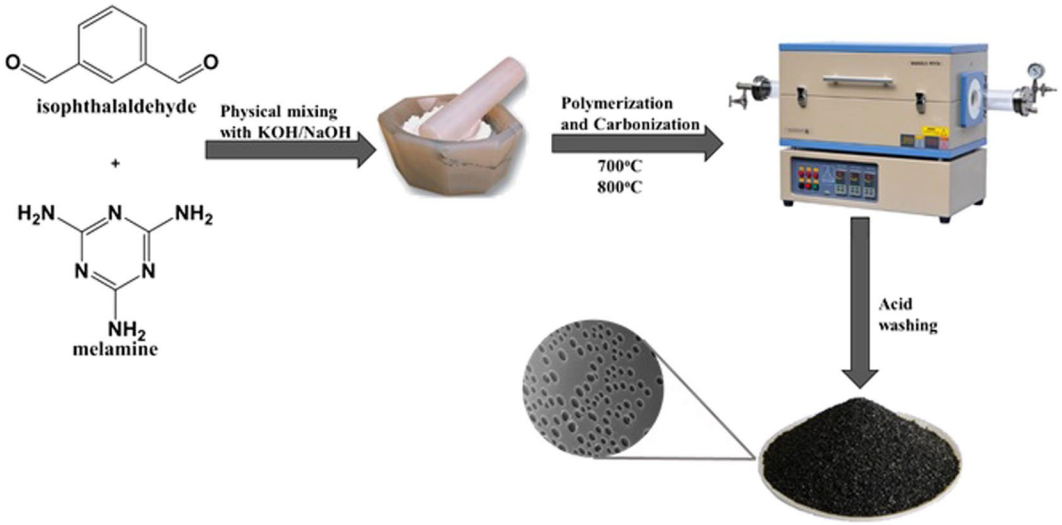

Figure 1. Synthetic procedure for activated microporous carbons.

active intermediates[11]. However, experimental and theoretical data present a general reaction between carbon and KOH, as presented in Eq. (1).

$$6KOH + 2C \rightarrow 2K + 3H_2 + 2K_2CO_3 \quad (1)$$

KOH is entirely consumed when carbon is heated at ~600 °C. At temperatures higher than 700 °C, the as-formed K_2CO_3 starts to decompose into CO_2 and K_2O and finally vanishes at 800 °C. At temperatures above 700 °C, potassium compounds including K_2O and K_2CO_3 are reduced to metallic potassium, which remains embedded in the carbon matrix.

$$K_2CO_3 \rightarrow K_2O + CO_2 \quad (2)$$

$$CO_2 + C \rightarrow 2CO \quad (3)$$

$$K_2CO_3 + 2C \rightarrow 2K + 3CO \quad (4)$$

$$C + K_2O \rightarrow 2K + CO \quad (5)$$

According to the above discussions, the KOH activation mechanisms proposed are (a) Chemical activation by various potassium compounds involves the etching of carbon frameworks due to the redox reactions resulting in the generation of a porous network and (b) the intercalation of the metallic form of potassium into the carbon framework during the activation resulting in the expansion of this framework[12]. Activation followed by washing removes the intercalated metallic as well as other forms of potassium. As a result, the carbon framework remains expanded without reverting to its nonporous structure, and thus, high microporosity is generated. Sodium hydroxide is also widely used as activating agent. According to previous studies, anthracite NaOH activation significantly increases the surface area from 1017 to 2208 m^2/g and the micropore volume from 0.05 to 0.4 cm^3/g, with the NaOH to char ratio varying from 1 to 3[13]. However, at high ratios, the micropores enlarged into mesopores, owing to excessive NaOH etching. Moreover, these conventional methods of activation exhibit limitations in controlling the pore size and formation of bottlenecks and/or micropores, typically with a size below 0.7 nm. Contrary to this, one of the interesting synthetic protocol proposed recently involves the condensation and activation of polymer precursors in molten salt medium with these salts playing the role of an alternative solvent as well as porogen for designing porous carbons.

In this context, a direct synthetic strategy is reported for the one step polymerization, carbonization, and activation of the carbon precursors to produce microporous carbons. Two types of carbon materials were prepared at two different temperatures using KOH and a eutectic mixture of KOH-NaOH as the two molten salt media. The resulting carbon materials were evaluated in terms of their ability to serve as gas storage materials.

Results and Discussion

Porous materials are an emerging platform of scientific interest in the context of their applicability in gas storage, energy storage, and catalytic activities. The successful transformation of the monomers to microporous carbons (Fig. 1) is evident from FTIR spectra. Attenuation of the peak corresponding to the aldehyde at 1690 cm^{-1} as well as the appearance of weak signals at ~3410 cm^{-1} corresponding to the stretching vibration of secondary amine (N−H), and methylene (CH) at 2917 cm^{-1} as the remnants of aminal linkages are confirmation of polymerization of organic precursors (Fig. 2). In addition, the peak of the triazine ring is evident at 1556 cm^{-1}. The presence

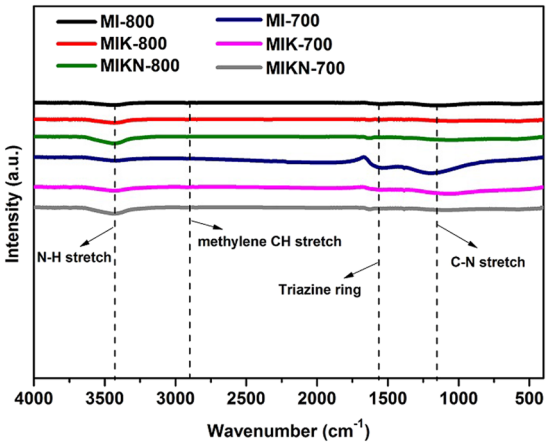

Figure 2. FTIR spectra of fabricated carbon materials.

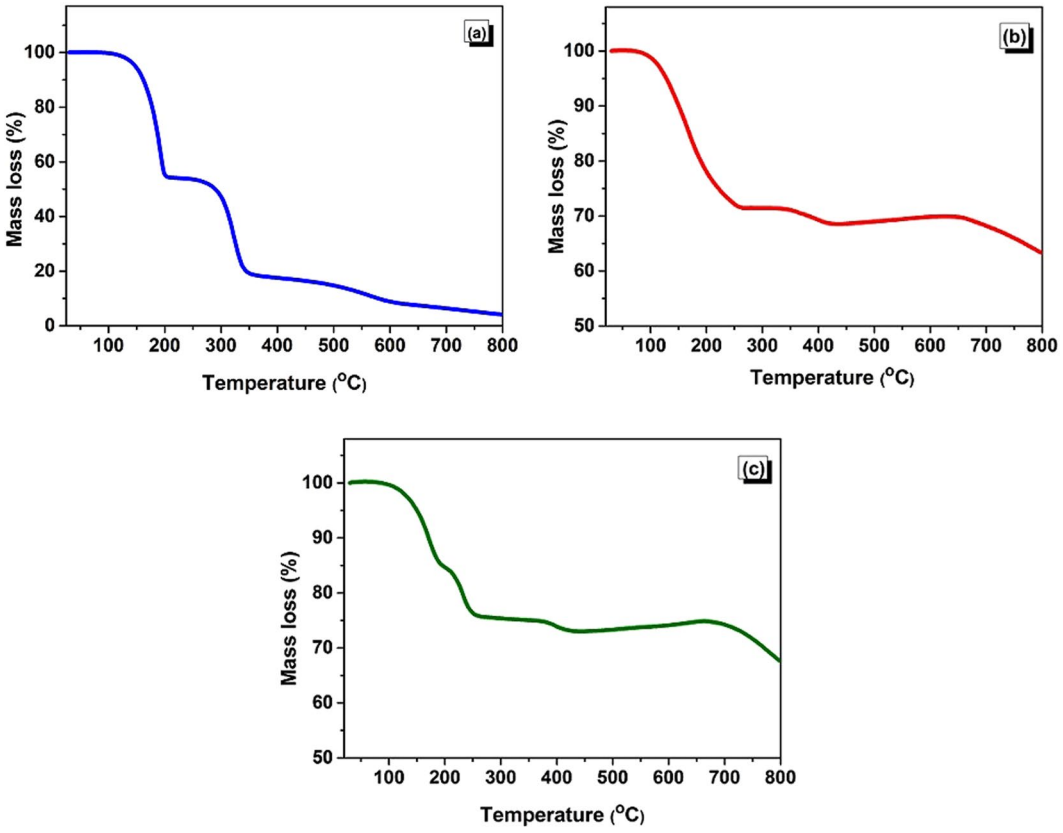

Figure 3. TGA thermograms of (**a**) MI (**b**) MIK and (**c**) MIKN before carbonization.

of a broad band at 978–1210 cm^{-1} is ascribed to the vinyl group (=C–H) and (C–N) bonds. The decrease in the intensity of the bands between 1000–1600 cm^{-1} suggest the removal of the O/C–H/C atomic species during carbonization. However, the absence of sharp peaks of any characteristic functionality indicates the effective carbonization of the polymer structure at the targeted temperatures. Moreover, the results indicate the leftovers of nitrogen functionalities which plays a vital role for enhancing CO_2 adsorption[13].

For a better understanding the effects of the activating agents on the polymerization–carbonization–activation processes, we analyzed the thermal stability of the precursors. Figure 3 presents the thermogravimetric (TG) analysis curves for the three samples (melamine + isophthalaldehyde (MI), melamine + isophthalaldehyde + KOH (MIK), and melamine + isophthalaldehyde + KOH + NaOH (MIKN)). An overlap is observed in the TG curves of the samples with KOH and eutectic KOH–NaOH mixture, indicating that a similar mechanism is involved in the weight loss in the course of one-pot processes. Moreover, it reveals that any dissimilarity in the microstructure of the activated carbonaceous materials are rather due to the physical state of the activating agent

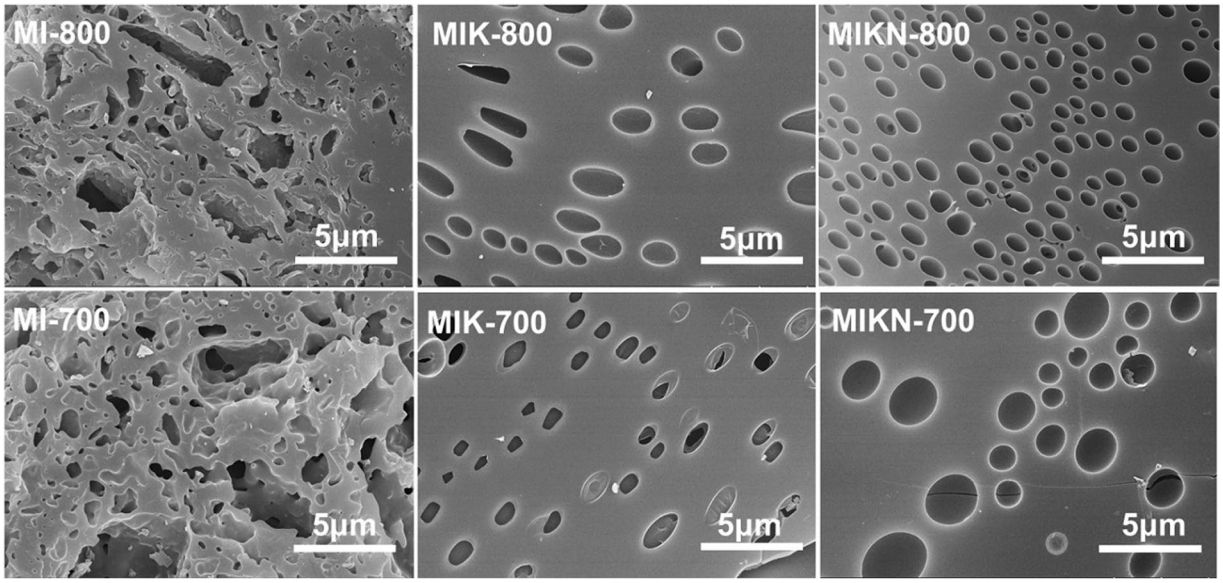

Figure 4. HR-SEM images of fabricated carbon materials.

during polymerization. Furthermore, eutectic mixture is the physical mixture of NaOH and KOH. The mixture is used for lowering the melting point of individual salt and thus provides a molten medium for monomers to condense at desired polymerization temperature. As anticipated, the sample with this eutectic mixture shows a rapid mass loss at temperatures below 200 °C, which is attributed to its low melting point. However, it should be noted that a strong mass loss that appeared at 346 °C in the TG curve of MI has disappeared in the curves of the sample mixtures with the activating agents. This is justified by the notable evolution of unreacted melamine in MI. Thus, the activating agents act as an efficient reaction media for the *in situ* polymerization in comparison to the hydroxide-free process. Subsequently, a progressive weight loss observed at temperatures above 600 °C is attributed to the carbonization of the polymer. The major component left behind is the carbon with traces of heteroatoms, as proved by elemental analysis. Henceforth, TG curves are used to explore the polymerization–carbonization processes occurring in the eutectic mixtures, resulting in the excellent yield of carbons.

SEM images (Fig. 4) clearly show that the carbons fabricated in the presence of hydroxide activating agents exhibit a different morphology than those prepared without them. MI-700 and MI-800 show rough surfaces formed by irregularly interconnected networks with voids, in accordance with their low specific surface areas. However, MIK-700 and MIK-800 exhibit smooth surfaces with some spherical voids. Apparently, polymerization occurred in the liquid media, and the polymer framework has the ability to entrap the generated bubbles released as reaction products or drops of the eutectic mixture. Hence, spherical voids formed in the carbonized material, as observed in the SEM images. Furthermore, MIKN-700 and MIKN-800 exhibit hierarchical porosity with a large number of mesopores. This is attributed to excessive NaOH etching in the eutectic mixture. The diffraction patterns (XRD) of all the carbon materials are presented in Figure S1. From the figure, it is revealed that washing remove all the impurities of sodium and potassium, as no crystalline peak was observed. Consequently, the only peaks observed were attributed to carbon-based materials with the graphitic nature. The diffraction peak of the (002) plane attributed to the periodicity in the ABAB hexagonal close packing of graphitic structures along the z-axis is absent in almost all the diffraction patterns. Apart from this, a high intense scattering peak is observed at low 2θ values, indicating the disorderness with a low stacking order in graphene sheets, possibly owing to the extensive micropore generation during the activation process.

X-ray photoelectron spectroscopy reveals the surface characteristics of prepared carbons. The survey scans (Fig. 5) show the presence of a high percentage of carbon along with a moderately low oxygen content. The high-carbon content reveals that the prepared sample mainly composed of carbon. The moderate to low nitrogen contents are in accordance with the elemental analysis data. Elemental analysis data (Table 1) indicates that the material contains mainly carbon with a small amount of nitrogen. A careful analysis of the consequences of the carbonization process reveals a large loss of mass with the release of large volumes of volatile gases and some tarry substances[14,15] and as a result, H and N contents decrease with an increase in the carbon content[16]. All the samples are rich in carbon because the process combined carbonization and activation. The carbon content of MIKN increased gradually from 75.9 to 90.6% as the temperature was increased to 700 to 800 °C, whereas the content of nitrogen decreases from 1.65 to 0.77%. The increase in the carbon content during the carbonization is attributed to two factors: (i) Increased formation of carbon basal planes and (ii) aromatization[17].

Physical properties including the textural features (specific surface area, pore-size distributions, and pore volumes) of the prepared materials were evaluated to assess their role in gas (CO_2 and H_2) adsorption. For this purpose, adsorption-desorption isotherms were obtained at 77 K. The isotherms and pore size distributions are presented in Fig. 6(a,b). The textural properties are summarized in Table 2. The adsorption profiles (Fig. 6a) of all the prepared samples indicate rapid uptake of nitrogen gas at low pressures with Type I adsorption characteristic,

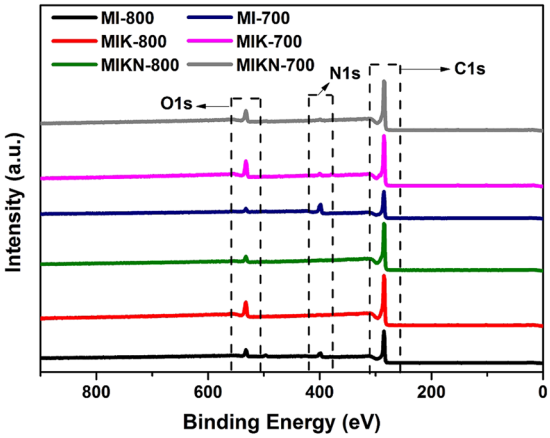

Figure 5. XPS survey scan of adsorbents prepared.

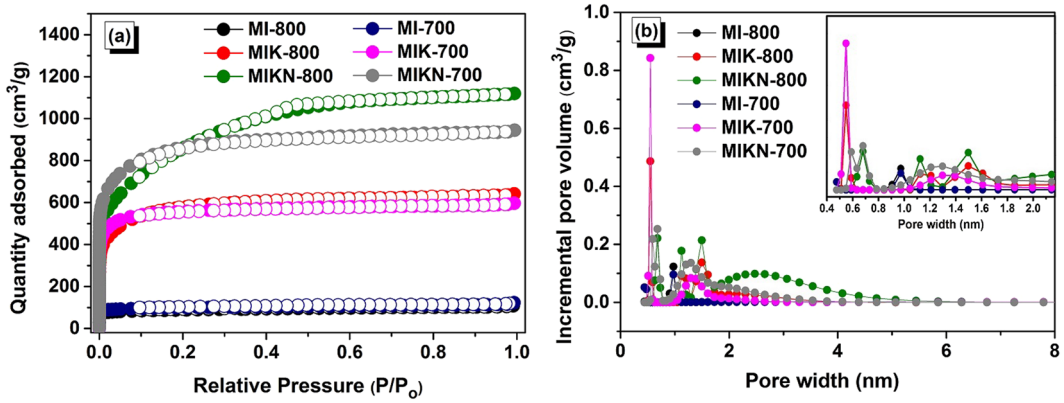

Figure 6. (**a**) Nitrogen adsorption-desorption isotherms and (**b**) pore size distributions of the adsorbents prepared.

Materials	Weight (%)		
	C content[a]	H content[b]	N content[c]
MI-800	67.84	0.56	12.57
MIK-800	85.98	0.21	0.76
MIKN-800	90.60	0.22	0.77
MI-700	64.32	0.70	21.65
MIK-700	67.42	0.66	2.66
MIKN-700	75.92	0.42	1.65

Table 1. Elemental composition of the adsorbents prepared. [a]Carbon content. [b]Hydrogen content. [c]Nitrogen content determined by the elemental analysis.

according to the IUPAC classification[18]. This kind of isotherm indicates a high affinity of the adsorbate and adsorbent for each other, and also suggests that the adsorbent in question is comprised mainly of micropores. However, MIKN-700 and MIKN-800 exhibit both Type I and Type IV isotherms. The isotherms exhibit nitrogen uptake at high pressures, indicating the presence of medium-sized or large mesopores along with the micropores. Furthermore, upon comparison of specific surface areas it is revealed that the initial blank samples, MI-700 and MI-800, prepared without any hydroxide activating agent exhibit a moderately low surface area of 330 and 360 m^2/g, respectively, which is still better than those of the samples prepared by the old conventional synthesis methods[8,9,19]. Samples synthesized in the presence of KOH only, MIK-700 and MIK-800, possess a high surface area of 2101 and 2090 m^2/g, respectively. This could be because the KOH activation leads to the generation of micropores primarily, resulting in a higher micropore volume and hence a porous carbon with a higher surface area[20]. On the other hand, samples prepared with the KOH-NaOH mixture, MIKN-700 and MIKN-800, leads to the generation of a hierarchical porous structure with both meso- and micropores with the surface areas of 3246 and 2984 m^2/g, respectively. It is worth noting that with an increase in the carbonization temperature, hierarchical

Materials	S_{BET}[a] (m^2/g)	V_{total}[b] (cm^3/g)	V_{micro}[c] (cm^3/g)	V_{meso}[d] (cm^3/g)	V_{micro}/V_{total} (%)	D_{pore}[e] (nm)
MI-800	330	0.20	0.16	0.04	80	6.85
MIK-800	2090	1.31	0.02	1.28	1.5	1.20
MIKN-800	2984	1.98	0.07	1.89	3.5	1.95
MI-700	360	0.26	0.21	0.04	80.7	5.05
MIK-700	2101	1.39	1.33	0.05	95.6	1.05
MIKN-700	3246	1.79	1.58	0.20	88.2	1.24

Table 2. Textural properties of the adsorbents prepared. [a]Surface area calculated by BET method. [b]Total pore volume determined at $P/P_o = 0.98$. [c]Micropore volume. [d]Mesopore volume. [e]Maxima of the pore size distribution determined by the NLDFT method.

meso- and microporosity is induced with higher mesopore volume and wider pore size diameter. This can be explained by the decomposition mechanism of salts which upon high temperature reduces to metallic species (sodium and potassium). With the passage of time, a portion of metallic species tends to evaporate from the lattice. However, some proportion of it remains intercalated. Consequently, all these phenomena generate a hierarchical meso- and microporous structure. However, all the superactivated microporous structures were prepared with the mass ratio of 2/1 between the activating agents and monomers. The specific surface area and adsorption profiles of MIK and MIKN are better than those of the materials obtained by chemical activation at high activating agent/precursor ratios[21]. On comparison with the single salt activation method, MIKN-700 exhibit excellent textural features than UAK2–800[20]. Similarly, UANa-960p presents a method with use of 3:1 activating agent to carbon precursor ratio[13]. However, in our work we used lesser amount of activating agents (2:1) with excellent results. Present method generates microporous carbon structure with high specific surface area and narrow pore size diameters. This is accredited to the use of KOH-NaOH eutectic mixture rather than single salt activation. Hence, it is claimed that the present strategy provides a facile way to design highly microporous carbons.

The micropore volumes of the prepared samples were estimated using the Dubinin–Radushkevich (D–R) equation shown below:

$$W = W_o exp\left[-B\left(\frac{T}{\beta}\right)Log^2\left(\frac{P}{P_o}\right)\right]$$

where, W indicates the amount of the liquid adsorbed at P/P_0, W_0 is the total amount of the adsorbate in the micropores, B is the adsorbent constant, and β represents the affinity coefficient (0.34 for N_2)[22]. The ratio of the micropore volume to total volume turns out to be 80, 1.5, 3.5, 80.7, 95.6, and 88.2% for MI-800, MIK-800, MIKN-800, MI-700, MIK-700, and MIKN-700, respectively. The samples prepared at 700 °C possesses a higher micropore volume compared to that prepared at 800 °C, suggesting that the activation at higher temperature is detrimental for the generation of micropores; instead, it stimulates the formation of mesopores. Similar outcomes were observed by Prahas *et al.* who reported that the elevation of the activation temperature drive the widening of the micropores into mesopores[23].

To investigate the textural parameters deeply, pore size distribution curves were obtained by the nonlocal density functional theory (NLDFT). Figure 6(b) illustrates the pore size distributions of all the prepared samples. The pore size of the samples prepared in the presence of molten salts lies in the range of 0.5 and 3 nm. In contrast, MI possesses mesopores in combination with micropores, and therefore, the average pore size of these samples lies at ~6 nm. It is well known phenomenon that the pore size less than 1 nm is highly beneficial for gas adsorption and storage. Consequently, samples with micropores of an optimum pore size can be employed as efficient candidates for gas adsorption[24].

At pressures up to 1 bar, the CO_2 adsorption isotherms obtained at 273, 283, and 298 K, respectively, are presented in Fig. 7 and the complete adsorption data is listed in Table 3. At 1 bar and 273 K, microporous carbons exhibit an excellent CO_2 uptake of 9.7 mmol/g (429.6 mg/g), 8.9 mmol/g (392.1 mg/g), 8.3 mmol/g (368.4 mg/g), 7.5 mmol/g (333.1 mg/g), 3.1 mmol/g (137.6 mg/g), and 2.9 mmol/g (130.1 mg/g), respectively, for MIK-700, MIK-800, MIKN-700, MIKN-800, MI-700, and MI-800, which are comparable to the CO_2 uptake of recently reported CO_2 adsorbents (Table 4). The CO_2 adsorption isotherms of all the sorbents are nonlinear, indicating their microporous nature. All the prepared samples suffered a clear loss in the CO_2 uptake with an increase in temperature from 273 to 298 K. This trend is in accordance with the exothermic nature of the adsorption process, implying that the amount of adsorbed CO_2 decreases with an increase in the temperature[25]. One of the representative samples exhibits a CO_2 uptake of 9.7 mmol/g (429.6 mg/g) at 273 K which decreases to 7.0 mmol/g (312.2 mg/g) and 5.4 mmol/g (238.7 mg/g) at 283 and 298 K, respectively.

Furthermore, the relationship between the CO_2 adsorption ability and the textural properties of the activated carbons materials was evaluated. From the textural studies it is revealed that the samples prepared in the presence of KOH exhibit well-defined micropores with a higher micropore volume and narrower pore size distribution. More specifically, MIK-700 and MIK-800 exhibit narrow pore sizes, suggesting that the contribution of narrow micropores to the adsorption capacity is greater than those of the wider micropores and mesopores. This is because, in low pressure studies, these narrow micropores are easily filled by the CO_2 molecules with a greater adsorption potential compared to wider pores. Furthermore, the higher activation temperature (MIKN-800) and presence of NaOH (MIKN-800 and MIKN-700) lead to wider micropores: 1.95 nm for MIKN-800 and 1.79 nm for MIKN-700. Consequently, there is an increase in the specific surface area and pore volume (2984 m^2/g and

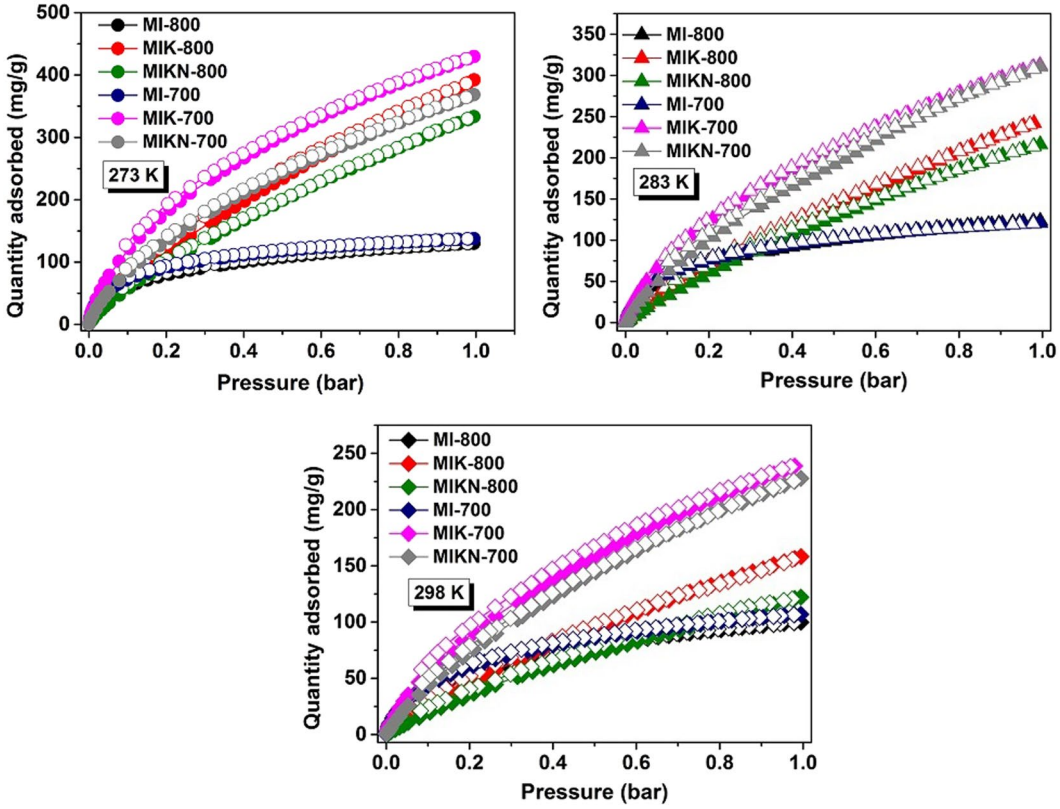

Figure 7. CO_2 adsorption-desorption isotherms.

Materials	CO_2 uptake			Q*st* (kJ/mol)	H_2 uptake wt. (%) 77 K
	273 K (mg/g)	283 K (mg/g)	298 K (mg/g)		
MI-800	130.1	123.4	99.0	34.6	0.95
MIK-800	392.1	343.9	158.2	31.6	3.1
MIKN-800	333.1	216.4	122.2	33.5	4.0
MI-700	137.6	120.7	106.9	37.9	0.98
MIK-700	429.6	312.2	238.7	38.2	2.58
MIKN-700	368.4	310.7	227.7	40.5	3.07

Table 3. CO_2 and H_2 adsorption capacities along with the isosteric heats of adsorption (Q*st*) for CO_2 gas determined at 273 and 283 K, shown by the prepared microporous carbons.

Materials	CO_2 Uptake (mmol/g)	References
MIK-700	**9.7**	**Present work**
MIK-800	**8.9**	**Present work**
Petroleum pitch	8.6	[48]
Petroleum coke	6.1	[49]
Polypyrrole	4.3	[50]
Bamboo-3-873	7.0	[51]
MAC	6.0	[52]
NC-650-3	7.0	[53]
SNU-C1-va	3.49	[54]
CS-6-CD-8	8.05	[55]
Microporous organic polymer	3.63	[56]
SG–MOP-5	3.37	[57]

Table 4. Comparison of CO_2 uptake by various adsorbents at 273 K and 1 bar.

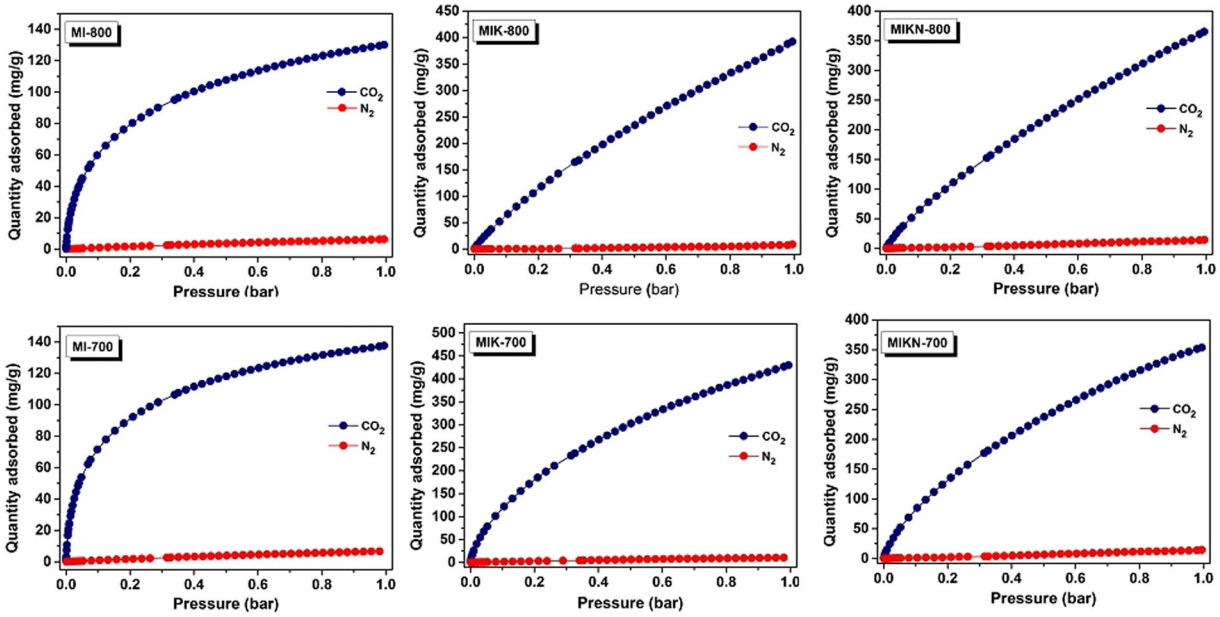

Figure 8. CO_2 and N_2 adsorption isotherms obtained at 273 K for selectivity measurements.

1.98 cm^3/g for MIKN-800 and 3246 m^2/g and 1.79 cm^3/g for MIKN-700, respectively) but they contributed less to CO_2 adsorption at the atmospheric pressure because no pore filling occurred in these cases. It has been reported that narrow micropores play a crucial role in CO_2 adsorption[26,27]; however, the correlation between the pore size and CO_2 adsorption has been rarely investigated. Presser *et al.* reported a perfectly linear relationship between the pore structure (with pore diameter of <0.8 nm) and CO_2 uptake at 1 bar for carbide-derived carbons[28]. Apart from a suitable texture, MIK-700 also possesses higher nitrogen content (2.66%) compared to other samples prepared in molten salt media. This can improve the Lewis acid-base interactions between CO_2 molecules and nitrogen moieties, leading to efficient adsorption. Consequently, the results confirm that the fabrication of efficient CO_2 carbon sorbents requires a precise control of the porosity, with a pore size of approximately 1 nm along with the hetero-atom doping.

Easy regeneration is another critical feature that must be considered while designing CO_2 sorbents. In this respect, porous carbons offer certain advantages over other materials, such as zeolites. The isosteric heat of adsorption (ΔH_{ads} or Q*st*) was calculated on the basis of the Clausius−Clapeyron equation shown below.

$$\ln\left(\frac{P_2}{P_1}\right) = -\frac{\Delta H_{ads}}{R}\left(\frac{1}{T_2} - \frac{1}{T_1}\right)$$

where, P_2 and P_1 are the values of $p(CO_2)$, R denotes the universal gas constant, and T_2 and T_1 are 273 and 283 K, respectively. Figure S2 shows the Q_{st} values as a function of adsorbed CO_2; the corresponding data is listed in the Table 3. The initial values of Q_{st} are in the range of 31.6–40.5 kJ/mol at a low surface coverage. However, the values show a decreasing trend with an increase in the amount of adsorbed gas, indicating that the interactions between CO_2 and the pore walls are stronger than those between the CO_2 molecules. The *Qst* values for the prepared samples are comparable to those of the nitrogen-doped templated carbons from zeolite and mesoporous silica (31−36 kJ/mol)[29,30], nitrogen-incorporated hierarchical porous carbons (33−37 kJ/mol)[31,32], and triptycene-derived benzimidazole-linked polymers (29 kJ/mol)[33]. This implies that the adsorption is physical in nature, which strongly depends on the pore structure of porous carbons. If Q*st* is too large, the regeneration of the sorbents becomes too costly, and if it is too small, the CO_2 uptake and CO_2 selectivity over N_2 selectivity will be too small[34]. However, while choosing a suitable adsorbent material, the absolute uptake of CO_2 is not the only factor to be considered; selectivity over other competing gases and particulates is also an important feature. For a material showing excellent adsorption profile for pure CO_2 gas but simultaneously adsorbing a large amount of another gas in a more realistic gas mixture, the working capacity would be dramatically reduced. Ideally, CO_2 adsorbents must exhibit a selective adsorption behavior over all other sorbates. For this reason, CO_2/N_2 selectivity studies were performed at 273 K. Selective adsorption behaviors of the adsorbents can be well-explained from the view point of molecular sieving, which demonstrates that kinetic diameters plays a dominant role during the gas adsorption. The kinetic diameters of CO_2 and N_2 are 3.30 and 3.64 Å, respectively, as reported earlier[35]. Hence, owing to the small diameter, CO_2 is adsorbed more than N_2. Apart from this, another factor to be considered is the thermodynamics, emphasizing the role of the critical temperature of the two gases in the selective adsorption behavior. The critical temperatures (T_c) of gaseous CO_2 and N_2 are reported to be 304.2 and 126.2 K, respectively. As CO_2 has a higher critical temperature, CO_2 molecules easily condense and adsorb on the porous framework. The selectivities for CO_2 over N_2 (Fig. 8) determined by initial slope method comes out to be 238, 141, 53, 230,

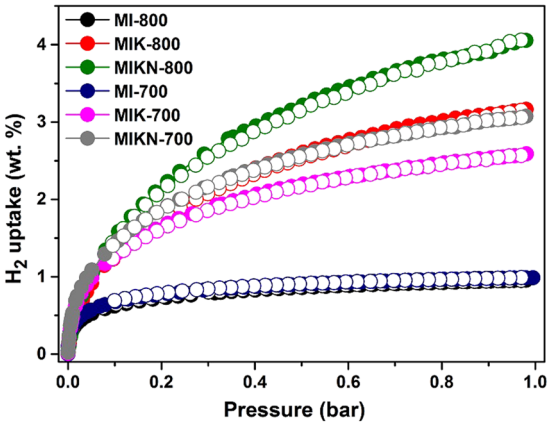

Figure 9. Hydrogen adsorption-desorption isotherms obtained at 77 K up to 1 bar.

111, and 71 at 273 K for MI-800, MIK-800, MIKN-800, MI-700, MIK-700, and MIKN-700, respectively, which are comparable to those of highly selective CO_2 adsorbents[36–38].

The hydrogen adsorption isotherms obtained at 77 K and 1 bar are presented in Fig. 9 and the details are listed in Table 3. The adsorption capacity can be enhanced either by increasing the storage pressure or decreasing the adsorption temperature to 77 K. Here, we chose a low temperature adsorption phenomenon. All the isotherms are Type I (Langmuir-type) isotherms, demonstrating that the formation of a hydrogen monolayer results in a saturation condition which is a usual characteristic for microporous surfaces. However, with an increase in the pressure up to 1 bar, the gas uptake increases continuously but a clear plateau does not appear because of the low pressure measurements. Sample MIKN-800 shows the highest hydrogen storage capacity, reaching up to 4.0 wt% at 1 bar, which is attributed to its highest surface area as well as the maximum pore volume. The present work demonstrates a high performance than the previously reported data, 2.4 wt% for AX21[39], 2.8 wt% for activated carbons[40], 2.0 wt% for corncob[41], 2.6 wt% for wood[42], and 2.7 wt% for Quercus agrifolia-based ACs[43]. Additionally, MIKN-800 outperforms many MOFs and POPs in terms of its ability to store hydrogen gas at 77 K. This is due to high surface area with optimum pore structure, narrow pore-diameter with hierarchical meso-micro and ultra-micropores as well as nitrogen-doping. Heteroatom doping shows beneficial impact on gas storage property, as already reported in literature[44,45]. Moreover, samples MI-700 and MI-800 have the lowest surface areas and pore volumes and exhibit the lowest H_2 uptake of 0.95 wt%. Based on these results, we conclude that good correlation exists between the textural features (surface area and pore volume) and gas adsorption capacity of the carbons[46,47].

Conclusions

Sustainable microporous carbons were synthesized via a one-step condensation-activation strategy in the presence of molten salts. The hydroxide-containing molten salts are responsible for generating well-developed microporous structures with a high surface area. CO_2 and H_2 adsorption properties of the fabricated materials were investigated and the results reveal that the microporous carbons prepared using KOH at 700 °C exhibit an exceptionally high CO_2 adsorption (uptake = 9.7 mmol/g at 273 K and 1 bar). This outstanding CO_2 adsorption performance of the prepared carbons is principally attributed to the narrow micropores (1.05 nm) and ultimately the optimum micropore volume (1.33 cm^3/g). Similarly, the high specific area and pore volume contribute significantly to the H_2 storage performance at 77 K, with 4.0 wt% uptake of H_2 by MIKN-800 (specific surface area and pore volume of 2984 m^2/g and 1.98 cm^3/g, respectively). Hence, present work contributes an effort to design solvent-free single step strategy for high surface area containing microporous carbons as novel materials for efficient CO_2 and H_2 adsorption with an excellent CO_2/N_2 selective adsorption behavior.

Methods

Materials and synthesis. All the reagents comprising melamine (99%), isophthalaldehyde (99%), sodium hydroxide (98%), potassium hydroxide (95%), and hydrochloric acid were obtained from Sigma–Aldrich. In this study, melamine and isophthalaldehyde were carbonized to design two different types of porous carbons. The first, labeled as MIK-X, was synthesized using 1.24 g of melamine (M) with 1.36 g of isophthalaldehyde (I), and 5.0 g of KOH (K). All the reagents were mechanically ground and heated directly at 250 °C for 180 min followed by carbonization at the targeted temperature for 60 min with the heating rate of 1 °C min^{-1}. The resulting product was neutralized to pH 7 by washing sequentially with 3 M HCl solution and distilled water. The obtained material was allowed to dry overnight at 120 °C. The other sample is denoted as MIKN-X. The preparation was carried out following the same procedure described for MIK-X, except that the composition of the activating agents was 2.5 g KOH and 2.5 g NaOH (KN). For evaluating the role of molten salts, blank samples containing a mixture of melamine and isophthalaldehyde (MI-X) were prepared in the absence of the hydroxides. In the names of the prepared samples, X denotes the targeted temperature of carbonization (700 or 800 °C).

Physicochemical characterization. The synthesized carbon materials were characterized by different analytical techniques. FTIR spectra of the fabricated samples were collected between 4000−400 cm^{-1} using a Fourier

transform-infrared vacuum VERTEX 80 V spectrometer. A thermal gravimetric analyzer (TGA; TG209F3) determined the thermal stability of the prepared materials under nitrogen atmosphere. X-ray diffraction patterns were recorded on a D2 PHASER, BRUKER, X-ray diffractometer. All the recordings were made in the range of 2° to 80° (*2θ*). For exploring the morphological structures, field emission scanning electron microscopy (FESEM; Model SU8010, Hitachi Co., Ltd.) was used. Elemental analysis was performed using an EA1112 element analyzer. Further surface characterization was performed by X-ray photoelectron spectroscopy using XPS, VG Scientific Co., ESCA LAB MK-II. The textural features of the prepared materials were determined by obtaining N_2 adsorption−desorption isotherms from a Model Belsorp Max instrument (BEL Japan, Inc.). Carbon dioxide adsorption capacity at 273, 283, and 298 K and hydrogen storage at 77 K were determined by a Model Belsorp Max instrument (BEL Japan, Inc.). For the CO_2/N_2 selectivity measurements, adsorption measurements for both the gases were carried out at 273 K using a Model Belsorp Max instrument (BEL Japan, Inc.). Prior to all the adsorption measurements, the fabricated materials were stored under vacuum conditions by heating at 120 °C for 8 h.

References

1. Nugent, P. *et al*. Porous materials with optimal adsorption thermodynamics and kinetics for CO_2 separation. *Nature* **495**, 80–84 (2013).
2. Haszeldine, R. S. Carbon capture and storage: how green can black be? *Science* **325**, 1647–1652 (2009).
3. Wang, J. & Kaskel, S. KOH activation of carbon-based materials for energy storage. *J. Mater. Chem.* **22**, 23710–23725 (2012).
4. Kim, B. J., Lee, Y. S. & Park, S. J. Novel porous carbons synthesized from polymeric precursors for hydrogen storage. *Int. J. Hydrog. Energy* **33**, 2254–2259 (2008).
5. Lee, J., Kim, J. & Hyeon, T. Recent progress in the synthesis of porous carbon materials. *Adv. Mater.* **18**, 2073–2094 (2006).
6. Gu, W. & Yushin, G. Review of nanostructured carbon materials for electrochemical capacitor applications: advantages and limitations of activated carbon, carbide-derived carbon, zeolite-templated carbon, carbon aerogels, carbon nanotubes, onion-like carbon, and graphene. *WIREs Energy and Environment* **3**, 424–473 (2014).
7. Kim, K. S. & Park, S. J. Synthesis and high electrochemical capacitance of N-doped microporous carbon/carbon nanotubes for supercapacitor. *J. Electroanal. Chem.* **673**, 58–64 (2012).
8. Schwab, M. G. *et al*. Catalyst-free preparation of melamine-based microporous polymer networks through Schiff base chemistry. *J. Am. Chem. Soc.* **131**, 7216–7217 (2009).
9. Rehman, A. & Park, S. J. Influence of nitrogen moieties on CO_2 capture by polyaminal-based porous carbon. *Macromol Res.* **25**, 1035–1042 (2017).
10. Meng, L. Y. & Park, S. J. Effect of heat treatment on CO_2 adsorption of KOH-activated graphite nanofibers. *J. Colloid Interface Sci.* **352**, 498–503 (2010).
11. Romanos, J. *et al*. Nanospace engineering of KOH activated carbon. *Nanotechnology* **23**, 015401 (2011).
12. Lee, S. Y. & Park, S. J. Determination of the optimal pore size for improved CO2 adsorption in activated carbon fibers. *J. Colloid Interface Sci.* **389**, 230–235 (2013).
13. Lillo-Ródenas, M., Lozano-Castelló, D., Cazorla-Amorós, D. & Linares-Solano, A. Preparation of activated carbons from Spanish anthracite: II. Activation by NaOH. *Carbon* **39**, 751–759 (2001).
14. Karacan, I. & Erzurumluoğlu, L. The effect of carbonization temperature on the structure and properties of carbon fibers prepared from poly (m-phenylene isophthalamide) precursor. *Fiber Polym.* **16**, 1629–1645 (2015).
15. Suárez-García, F., Villar-Rodil, S., Blanco, C., Martínez-Alonso, A. & Tascón, J. Effect of phosphoric acid on chemical transformations during Nomex pyrolysis. *Chem. Mater.* **16**, 2639–2647 (2004).
16. Garlapalli, R. K., Wirth, B. & Reza, M. T. Pyrolysis of hydrochar from digestate: Effect of hydrothermal carbonization and pyrolysis temperatures on pyrochar formation. *Bioresour Technol.* **220**, 168–174 (2016).
17. Fierro, V., Torné-Fernández, V. & Celzard, A. Kraft lignin as a precursor for microporous activated carbons prepared by impregnation with ortho-phosphoric acid: synthesis and textural characterisation. *Microporous Mesoporous Mater.* **92**, 243–250 (2006).
18. Sing, K. Reporting physisorption data for gas/solid systems with special reference to the determination of surface area and porosity (Provisional). *Pure Appl. Chem.* **54**, 2201–2218 (1982).
19. He, B., Li, W. C. & Lu, A. H. High nitrogen-content carbon nanosheets formed using the Schiff-base reaction in a molten salt medium as efficient anode materials for lithium-ion batteries. *J. Mater. Chem. A* **3**, 579–585 (2015).
20. Lozano-Castello, D., Lillo-Rodenas, M., Cazorla-Amorós, D. & Linares-Solano, A. Preparation of activated carbons from Spanish anthracite: I. Activation by KOH. *Carbon* **39**, 741–749 (2001).
21. Su, S., Lai, Q. & Liang, Y. Schiff-base polymer derived nitrogen-rich microporous carbon spheres synthesized by molten-salt route for high-performance supercapacitors. *RSC Adv.* **5**, 60956–60961 (2015).
22. Misra, D. N. Adsorption on heterogeneous surfaces: A dubinin-radushkevich equation. *Surf. Sci.* **18**, 367–372 (1969).
23. Prahas, D., Kartika, Y., Indraswati, N. & Ismadji, S. Activated carbon from jackfruit peel waste by H_3PO_4 chemical activation: pore structure and surface chemistry characterization. *Chem. Eng. J.* **140**, 32–42 (2008).
24. Yoo, H. M., Lee, S. Y. & Park, S. J. Ordered nanoporous carbon for increasing CO_2 capture. *J. Solid State Chem.* **197**, 361–365 (2013).
25. Hedin, N., Andersson, L., Bergström, L. & Yan, J. Adsorbents for the post-combustion capture of CO_2 using rapid temperature swing or vacuum swing adsorption. *Appl Energ.* **104**, 418–433 (2013).
26. Hu, X., Radosz, M., Cychosz, K. A. & Thommes, M. CO_2-filling capacity and selectivity of carbon nanopores: synthesis, texture, and pore-size distribution from quenched-solid density functional theory (QSDFT). *Environ. Sci. Technol.* **45**, 7068–7074 (2011).
27. Martin-Martinez, J., Torregrosa-Macia, R. & Mittelmeijer-Hazeleger, M. Mechanisms of adsorption of CO_2 in the micropores of activated anthracite. *Fuel* **74**, 111–114 (1995).
28. Presser, V., McDonough, J., Yeon, S.-H. & Gogotsi, Y. Effect of pore size on carbon dioxide sorption by carbide derived carbon. *Energy Environ. Sci.* **4**, 3059–3066 (2011).
29. Zhao, Y. *et al*. Novel porous carbon materials with ultrahigh nitrogen contents for selective CO_2 capture. *J. Mater. Chem.* **22**, 19726–19731 (2012).
30. Wang, L. & Yang, R. T. Significantly increased CO_2 adsorption performance of nanostructured templated carbon by tuning surface area and nitrogen doping. *J. Phys. Chem. C* **116**, 1099–1106 (2011).
31. Gutiérrez, M. C. *et al*. Deep eutectic solvents as both precursors and structure directing agents in the synthesis of nitrogen doped hierarchical carbons highly suitable for CO_2 capture. *Energy Environ. Sci.* **4**, 3535–3544 (2011).
32. Chen, C., Kim, J. & Ahn, W.-S. Efficient carbon dioxide capture over a nitrogen-rich carbon having a hierarchical micro-mesopore structure. *Fuel* **95**, 360–364 (2012).
33. Rabbani, M. G., Reich, T. E., Kassab, R. M., Jackson, K. T. & El-Kaderi, H. M. High CO2 uptake and selectivity by triptycene-derived benzimidazole-linked polymers. *ChemComm.* **48**, 1141–1143 (2012).
34. Chue, K., Kim, J., Yoo, Y., Cho, S. & Yang, R. Comparison of activated carbon and zeolite 13X for CO_2 recovery from flue gas by pressure swing adsorption. *Ind. Eng. Chem. Res.* **34**, 591–598 (1995).

35. Shin, G.-J., Rhee, K. & Park, S.-J. Improvement of CO_2 capture by graphite oxide in presence of polyethylenimine. *Int. J. Hydrog. Energy* **41**, 14351–14359 (2016).
36. Luo, Y., Li, B., Wang, W., Wu, K. & Tan, B. Hypercrosslinked aromatic heterocyclic microporous polymers: a new class of highly selective CO_2 capturing materials. *Adv. Mater.* **24**, 5703–5707 (2012).
37. Patel, H. A. *et al*. Directing the Structural Features of N_2-Phobic Nanoporous Covalent Organic Polymers for CO_2 Capture and Separation. *Chem. Eur. J.* **20**, 772–780 (2014).
38. Li, J.-R. *et al*. Porous materials with pre-designed single-molecule traps for CO_2 selective adsorption. *Nat. Commun.* **4**, 1538 (2013).
39. Texier-Mandoki, N. *et al*. Hydrogen storage in activated carbon materials: role of the nanoporous texture. *Carbon* **42**, 2744–2747 (2004).
40. Akasaka, H. *et al*. Hydrogen storage ability of porous carbon material fabricated from coffee bean wastes. *Int. J. Hydrog. Energy* **36**, 580–585 (2011).
41. Sun, Y. & Webley, P. A. Preparation of activated carbons from corncob with large specific surface area by a variety of chemical activators and their application in gas storage. *Chem. Eng. J.* **162**, 883–892 (2010).
42. Huang, C.-C., Chen, H.-M., Chen, C.-H. & Huang, J. C. Effect of surface oxides on hydrogen storage of activated carbon. *Sep. Purif. Technol.* **70**, 291–295 (2010).
43. Figueroa-Torres, M. Z., Robau-Sánchez, A., De la Torre-Sáenz, L. & Aguilar-Elguézabal, A. Hydrogen adsorption by nanostructured carbons synthesized by chemical activation. *Microporous Mesoporous Mater.* **98**, 89–93 (2007).
44. Parambhath, V. B., Nagar, R. & Ramaprabhu, S. Effect of nitrogen doping on hydrogen storage capacity of palladium decorated graphene. *Langmuir* **28**, 7826–7833 (2012).
45. Chen, L. *et al*. Facile synthesis and hydrogen storage application of nitrogen-doped carbon nanotubes with bamboo-like structure. *Int. J. Hydrog. Energy* **38**, 3297–3303 (2013).
46. Liu, X., Zhang, C., Geng, Z. & Cai, M. High-pressure hydrogen storage and optimizing fabrication of corncob-derived activated carbon. *Microporous Mesoporous Mater.* **194**, 60–65 (2014).
47. Lee, S. Y. & Park, S. J. Influence of the pore size in multi-walled carbon nanotubes on the hydrogen storage behaviors. *J. Solid State Chem.* **194**, 307–312 (2012).
48. Wahby, A. *et al*. High-Surface-Area Carbon Molecular Sieves for Selective CO_2 Adsorption. *ChemSusChem* **3**, 974–981 (2010).
49. Sevilla, M. & Fuertes, A. B. Sustainable porous carbons with a superior performance for CO_2 capture. *Energy Environ. Sci.* **4**, 1765–1771 (2011).
50. Chandra, V. *et al*. Highly selective CO_2 capture on N-doped carbon produced by chemical activation of polypyrrole functionalized graphene sheets. *ChemComm.* **48**, 735–737 (2012).
51. Wei, H. *et al*. Granular Bamboo-Derived Activated Carbon for High CO_2 Adsorption: The Dominant Role of Narrow Micropores. *ChemSusChem* **5**, 2354–2360 (2012).
52. Hao, W. *et al*. Correction to "High-Performance Magnetic Activated Carbon from Solid Waste from Lignin Conversion Processes. 1. Their Use As Adsorbents for CO_2". *ACS Sustain. Chem. Eng.* **5**, 7448–7448 (2017).
53. Chen, J. *et al*. Enhanced CO2 capture capacity of nitrogen-doped biomass-derived porous carbons. *ACS Sustain. Chem. Eng.* **4**, 1439–1445 (2016).
54. Xie, L. H. & Suh, M. P. High CO_2-Capture Ability of a Porous Organic Polymer Bifunctionalized with Carboxy and Triazole Groups. *Chem. Eur. J.* **19**, 11590–11597 (2013).
55. Wickramaratne, N. P. & Jaroniec, M. Activated carbon spheres for CO2 adsorption. *ACS Appl. Mater. Interfaces* **5**, 1849–1855 (2013).
56. Yao, S., Yang, X., Yu, M., Zhang, Y. & Jiang, J.-X. High surface area hypercrosslinked microporous organic polymer networks based on tetraphenylethylene for CO_2 capture. *J. Mater. Chem. A* **2**, 8054–8059 (2014).
57. Liu, F.-Q., Wang, L.-L., Li, G.-H., Li, W. & Li, C.-Q. Hierarchically structured graphene coupled microporous organic polymers for superior CO_2 capture. *ACS Appl. Mater. Interfaces* **9**, 33997–34004 (2017).

Acknowledgements

This research was supported by The Leading Human Resource Training Program of Regional Neo industry through the National Research Foundation of Korea(NRF) funded by the Ministry of Science, ICT and future Planning(grant number)(NRF-2016H1D5A1909732) and the Technological Innovation R&D Program (S2460853) funded by the Ministry of SMEs and Startups (MSS, Korea).

Author Contributions

A.R. designed, carried out the experiments, collected and analyzed the data, and wrote the manuscript. S.J.P. contributed to discuss the interpretation of the results and managed the overall execution of the project.

Additional Information

Supplementary information accompanies this paper at https://doi.org/10.1038/s41598-018-24308-z.

Competing Interests: The authors declare no competing interests.

Publisher's note: Springer Nature remains neutral with regard to jurisdictional claims in published maps and institutional affiliations.